Influence of the substrate characteristics on the bond behavior of PBO FRCM-concrete joints

Tommaso D'Antino [a,*], Lesley H. Sneed [b], Christian Carloni [c], Carlo Pellegrino [d]

[a] Department of Civil Engineering, University of Patras, Patras, Greece
[b] Department of Civil, Architectural and Environmental Engineering, Missouri University of Science and Technology, Rolla, MO, USA
[c] Department of Civil, Chemical, Environmental, and Materials Engineering, University of Bologna, Bologna, Italy
[d] Department of Civil, Architectural, and Environmental Engineering, University of Padova, Padova, Italy

Received 12 March 2015
Received in revised form 17 August 2015
Accepted 14 October 2015

1. Introduction

Fiber reinforced cementitious matrix (FRCM) composites represent a newly-developed promising alternative to traditional materials for strengthening and retrofitting reinforced concrete (RC) and masonry structures. They are comprised of high strength fibers embedded within an inorganic matrix that is responsible for the stress-transfer mechanism between the composite and the substrate. The fibers are usually bundled and arranged in a bidirectional net to improve the fiber–matrix bond characteristics. FRCM composites present several advantages with respect to fiber reinforced polymers (FRP) composites, e.g. the resistance to fire and high temperatures [1,2], resistance to UV radiation, ease of handling and application, and good compatibility with concrete and masonry substrates. While FRP composites have been extensively studied in the past several decades and several design guidelines and analytical formulations are available, FRCM composites are still in their infancy and limited results are available in the literature. FRCM composites have shown promise in flexural strengthening [3–7] and shear strengthening [8–11] applications, and confinement of axially and axially/eccentrically loaded elements [12–15].

* Corresponding author.
E-mail addresses: dantino@upatras.gr (T. D'Antino), sneedlh@mst.edu (L.H. Sneed), christian.carloni@unibo.it (C. Carloni), carlo.pellegrino@unipd.it (C. Pellegrino).

Nevertheless, design provisions and standard test methods for the characterization of these composites are still under discussion in the scientific community [3,16,17].

It is well known that the behavior of FRP-concrete joints is highly dependent upon the surface preparation and concrete substrate strength [18], with failure occurring within the concrete substrate [19]. On the other hand, the weakness of FRCM-concrete joints has been reported to be at the matrix–fiber interface [20–24], with failure characterized by increasing slippage of the fiber bundles with respect to the surrounding matrix [25–27]. The behavior of the composite is strongly influenced by the matrix–fiber interfacial bond, which in turn is affected by the capacity of the matrix to penetrate within the bundles impregnat-ing single fiber filaments [28]. Furthermore, the shape and spacing of the fiber net, as well as the preparation of the concrete surface and the strength of the concrete substrate, may also affect the behavior of the FRCM composite [29–31]. Since FRCM failure takes place within the composite, the substrate mechanical properties could be less significant than in FRP applications. If this assumption is confirmed, the experimental results obtained from FRCM-concrete joints may be extended to FRCM-masonry joints, provided that the weakness of FRCM-masonry joints is at the matrix–fiber interface [32].

In this paper the effect of surface preparation and concrete substrate strength is investigated experimentally through single-lap direct-shear tests of FRCM-concrete joints. The experimental campaign included 21 specimens presented in this paper supplemented with test results from additional specimens previously published by the authors [25–27]. The FRCM composite was comprised of a polyparaphenylene benzo-bisoxazole (PBO) fiber net embedded within a polymer-modified cement-based mortar. The concrete surface onto which the composite was applied was either sandblasted before the application or simply cleaned from dust and otherwise untreated. Concrete prisms with different strengths were used. Two different composite bonded lengths and different composite bonded widths were employed.

2. Background

Whereas failure of FRP-concrete joints is reported to be debonding within a thin mortar-rich layer of the concrete substrate [33], failure of FRCM-concrete joints is generally reported to be debonding of the fibers from the embedding matrix [20–27], although the type of composite, strengthening configuration, and method of application may lead to different failure modes. The bond behavior of PBO FRCM-concrete joints was studied by the authors by means of single-lap direct-shear tests. A sketch of the most common single-lap shear test set-up is illustrated in Fig. 1. Variations of the set-up have been used by several researchers [34]. The actual set-up used by the authors is discussed in Section 3.

Based on the analysis of a large number of experimental tests, the idealized load response of the PBO FRCM-concrete joint put forward by the authors [26,27] is shown in Fig. 2a. The idealized load response is described in terms of applied load P versus global slip g, where global slip is the slip of the fibers with respect to the concrete substrate at the loaded end of the composite [26,27]. It should be noted that the idealized load response depicted in Fig. 2a holds when the bonded length is longer than the effective bond length l_{eff}, i.e. the bonded length needed to fully develop the stress-transfer mechanism [26,35]. Similar to FRP-concrete joints, the applied load–global slip behavior of FRCM-concrete joints is characterized by an initial elastic branch up to the onset of micro-cracking at the fiber–matrix interface. When the applied load attains the load-carrying capacity (P_{deb} in Fig. 2) the stress-transfer mechanism is fully established, and the fibers start to debond from the embedding matrix at the loaded end. In the case of FRP-concrete joints, as the global slip increases after the onset of debonding the applied load remains constant, and the stress-transfer zone (STZ) self-similarly translates towards the free end [35]. It should be noted that in the case of FRP-concrete joints the failure could be brittle and sudden as the composite completely detaches from the substrate. In the case of FRCM-concrete joints, further increase of the global slip g after the onset of debonding results in an increase of the applied load due to the presence of friction (interlocking) between single fiber filaments and between fibers and matrix in the debonded region [26,27]. After the applied load reaches the peak load P^*, which corresponds to the condition where the residual bonded length is equal to the effective bond length, further increase of the global slip results in a decrease of the applied load until the constant load P_f due to friction is attained (Fig. 2). For illustration, the load response of specimen DS_330_80_D_1, previously reported by the authors [26] and rep-resentative of the load response observed in PBO FRCM-concrete joints, is depicted in Fig. 2b.

The effective bond length for FRP-concrete joints is the length of the STZ once it is fully established. It is computed as the difference between the coordinates of the points in the direction of the fibers where the strain is zero and where it reaches a constant value, i.e. where a strain plateau is observed. Alternatively, it is computed as the difference between the coordinates of the points in the direction of the fibers where the shear stress is zero. For FRCM-concrete joints the definition of the effective bond length requires some additional comments. In fact, because of the presence of fric-tion the strain profile does not reach a plateau. Hence, the effective bond length appears to increase as the STZ moves forward. How-ever, the apparent increase of the effective bond length is related to friction, which should not be considered if a cohesive interface is assumed [28,36]. Therefore, the effective bond length l_{eff} that characterizes FRCM-concrete joints can be computed from the strain distribution along the longitudinal fibers at the onset of debonding (applied load equal to P_{deb} in Fig. 2) or at applied load values between P_{deb} and P^*, provided that the contribution of fric-tion is clearly identified. l_{eff}, which was found to be 260 mm for the composite studied in this paper [26,27], can be defined as the smallest distance between the points of the strain distribution in which the derivative is equal to zero at the free end and the deriva-tive is constant at the loaded end. If the definition of the effective bond length is provided in terms of shear stress, it would result as the smallest difference between the points where the shear stress is zero at the free end and is constant at the loaded end. The value of l_{eff} = 260 mm found for this composite was confirmed by com-paring the peak stress from the load response of FRCM-concrete joints with different bonded lengths, including the results obtained by other authors [26].

As a first attempt to study the stress-transfer mechanism in FRCM-concrete joints, the fracture mechanics approach applied to FRP-concrete joints [33] was adopted in D'Antino et al. [26] and Carloni et al. [27]. The results obtained are briefly recalled

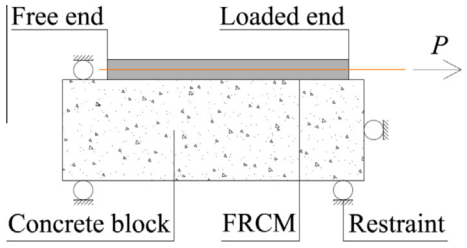

Fig. 1. Sketch of a single-lap direct-shear test set-up. Locations of the restraints can be varied.

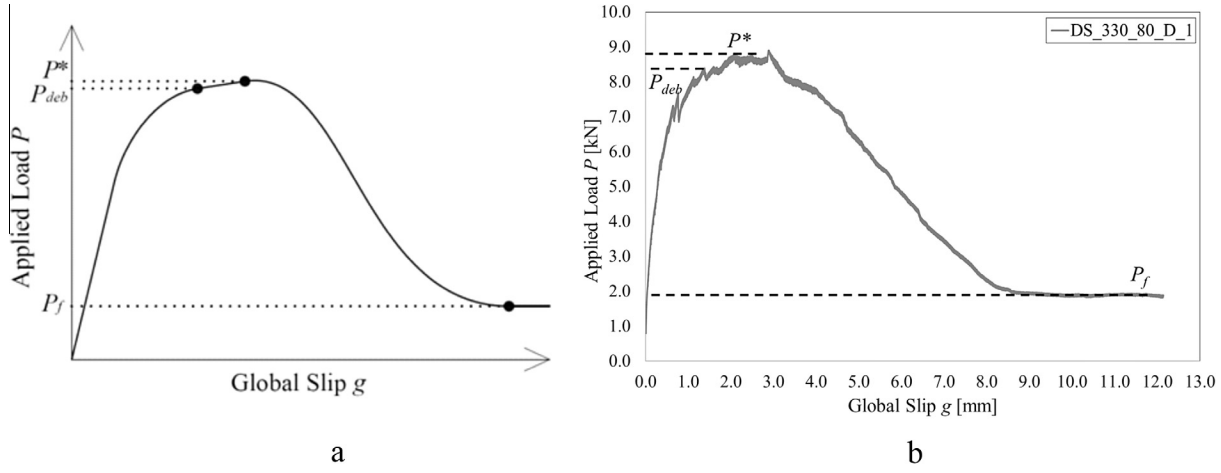

Fig. 2. (a) Idealized load response. (b) Load response of specimen DS_330_80_D_1 [26].

herein for the sake of clarity. For FRCM-concrete joints, it should be noted that two matrix–fiber interfaces exist. In fact, the fibers slip with respect to the internal matrix layer bonded to the concrete surface and with respect to the external matrix layer, which covers the fibers. The lateral surface of the fiber bundle is neglected. As a first attempt, it was assumed that the shear stresses at the internal and external interfaces are equal [26]. Assuming a Mode II loading condition at the matrix–fiber interface and neglecting the deformation of the concrete substrate and of the matrix, as confirmed by measurements of the matrix deformation field and by numeri-cal analysis [27,37], the interfacial shear stress τ corresponding to each matrix–fiber interface can be computed by Eq. (1):

$$\tau = \frac{1}{2} E t^* \frac{d\varepsilon}{dy} \tag{1}$$

where E is the elastic modulus of the fibers, ε is the strain of the fibers along the y (axial) direction, and t^* represents the thickness of a singular fiber bundle that is assumed to have rectangular cross-section with width b^* (note that t^* is not the nominal (equiv-alent) thickness of the textile). The interfacial slip s corresponding to the shear stress τ can be computed by integration of the fiber strain using Eq. (2):

$$s(y) = \int_0^y \varepsilon \, dy \tag{2}$$

where it was assumed that no slip occurred at the free end of the composite ($s(0) = 0$).

The strain profiles obtained by the authors on specimens equipped with strain gauges were employed to compute the shear stress–slip relationship that describes the stress-transfer mechanism at the matrix–fiber interface of PBO FRCM-concrete joints. The idealized τ–s curve proposed by the authors and the results obtained for specimen DS_330_60_S_2 [27] are shown in Fig. 3a and b, respectively.

With reference to the shear stress–slip relationship reported in Fig. 3, an infinitesimal segment of fibers debonds from the embedding matrix when the shear stress and the slip attain the values τ_f and s_f, respectively. If $s > s_f$, the fibers are debonded and the shear stress is due to friction (interlocking) only. As stated earlier, within a fracture mechanics approach friction should not be considered when the fracture energy is calculated. Thus the area under the shear stress–slip curve when $0 \leqslant s \leqslant s_f$ represents the fracture energy G_F (Fig. 3a). It should be noted that the contribution of friction between fiber filaments and between the longitudinal and transversal fiber bundles before the onset of debonding is included in the macro-fracture model [26] of the matrix–fiber interface put forward by the authors (Fig. 3). Further discussion about the maximum shear stress τ_{max}, the shear stress corresponding to friction τ_f, and the corresponding slip s_0 and s_f, respectively, that character-ize the matrix−fiber interface can be found in Carloni et al. [27].

The shear stress–slip relationship put forward by the authors (Fig. 3a) is valid until the stress-transfer mechanism is fully established. Among the reasons for this statement, it should be noted that when the STZ reaches the free end and its length is less than the effective bond length, the fracture process changes from predominately Mode II to a mixed Mode I + II. Thus, mixed-mode fracture propagation could occur toward the end of the test, which implies that the shear stress–slip relationship changes [38]. Although the idealized shear stress–slip relationship shown in Fig. 3a is able to predict the experimental load response up to the peak load P^*, as numerically described in [39,40], it is not able to reproduce accurately the post-peak load response. This aspect will be further investigated in a future publication when measurements of the free end slip will be available.

The load response and the shear stress–slip relationship shown in Figs. 2 and 3, respectively, were determined for FRCM-concrete joints in which the concrete surface was sandblasted before applying the composite, as is recommended for FRP-concrete joints [18]. Also, the potential influence of concrete substrate strength is unknown. In this paper, the effects of surface preparation and concrete mechanical properties is investigated by examining whether and how these variables influence the failure mode, load response, and peak load of FRCM-concrete joints.

3. Materials and methods

The FRCM composite employed was comprised of a bidirectional unbalanced PBO fiber net with rovings spaced at 10 and 20 mm on center in the two directions. The total weight per unit area of fibers in the net was 88.0 g/m^2, with 70.2 g/m^2 in the longitudinal and 17.8 g/m^2 in the transversal directions, respectively. The bundle thickness t^* was computed from the equivalent thickness reported by the manufacturer and was equal to 0.092 mm, and the measured width b^* of a single bundle was equal to 5 mm. The PBO bare fibers were subjected to tensile tests according to ASTM D3039 [41] to determine the tensile strength and elastic modulus. Seventeen specimens of fiber net with different number of bundles were tested [42]. At least two 50 × 100 mm cylinders were cast from each batch of mortar used to cast the FRCM composites and were tested to determine the matrix compressive strength and splitting tensile strength in accordance with ASTM C39 [43] and ASTM C496 [44]. Concrete prisms (blocks) with different concrete strengths were employed. Six 100 × 200 mm concrete cylinders were cast from each batch of concrete used to cast the blocks and were tested to determine the concrete compressive strength and splitting tensile strength in accordance with ASTM C39 [43] and ASTM C496 [44]. The mechanical properties of all materials tested are summarized in Table 1. The FRCM composite was applied onto the surface of the concrete blocks. The concrete blocks had a 125 × 125 mm cross-section and two different lengths L (Fig. 4), namely 375 mm and 510 mm (Table 2), depending on the composite

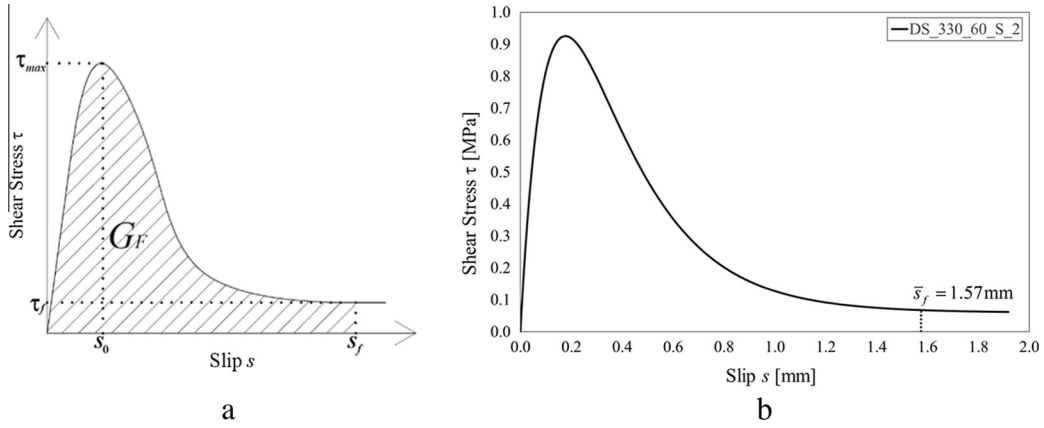

Fig. 3. (a) Idealized shear stress–slip curve. (b) Shear stress–slip curve of specimen DS_330_60_S_2 [27] obtained using Eqs. (1) and (2) applied to the strain profiles.

Table 1
Material properties.

	f_c [MPa] (CoV)	f_t [MPa] (CoV)	E [GPa] (CoV)
Concrete batch A	42.5 (0.013)	3.4 (0.113)	–
Concrete batch B	33.5 (0.085)	3.0 (0.042)	–
Concrete batch C	26.9 (0.026)	–	–
Mortar	28.4 (0.092)	3.5 (0.231)	–
PBO fiber	–	3014 (0.068)	206 (0.065)

Note: f_c = average compressive strength; f_t = average splitting tensile strength or average tensile strength; E = average elastic modulus.

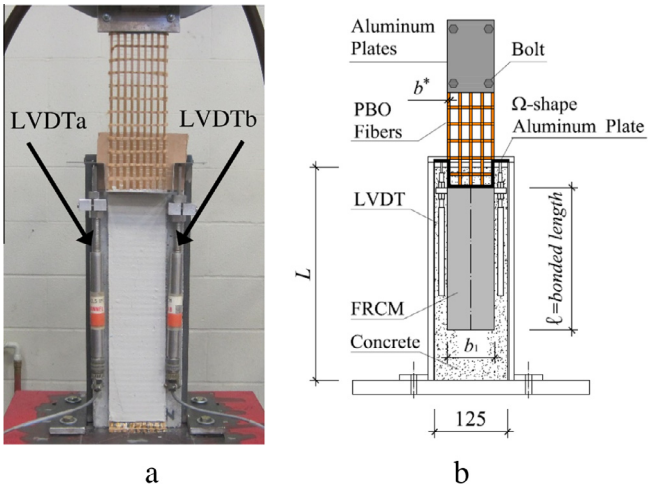

Fig. 4. (a) Photo of specimen DS_330_80_U_1. (b) Test set-up (Note: dimensions in mm).

bonded length. The matrix was applied to the concrete surface using molds to control the bonded area and the thickness of the matrix layers [25]. Only the formed faces of the blocks were employed. After the first (internal) 4 mm thick layer of matrix was applied, the fiber net was delicately pushed onto it to assure proper impregnation and then covered by a second (external) 4 mm thick layer of matrix. The composite was bonded starting at a distance of 38 mm from the prism edge at the loaded end. The fibers were left bare outside the bonded area. Two different bonded widths b_1 equal to 60 mm and 80 mm, corresponding to 7 and 9 longitudinal fiber bundles, respectively, were considered for the specimens first presented in this paper. For each bonded width two different bonded lengths ℓ were adopted, namely 330 mm and 450 mm (Table 2).

Single-lap direct-shear tests were conducted using the classical pull–push configuration where the concrete block was restrained while the fibers were pulled [33]. Aluminum plates were through-bolted and epoxy bonded to the end of the bare fibers to improve gripping. The concrete blocks were restrained by a steel frame bolted to the base of a servo-hydraulic universal testing machine (Fig. 4). Two LVDTs were mounted on the sides of the FRCM composite at the loaded end. The LVDTs reacted off of a thin aluminum Ω-shaped plate bonded to the bare fibers immediately outside the bonded length (Fig. 4). The average displacement measured by the LVDTs, taken as the global slip g, was used to control the tests that were conducted at the constant rate of 0.00084 mm/min. The tests were conducted until a certain value of the global slip was attained, typically 5 mm and 6 mm for specimens with bonded length equal to 330 mm and 450 mm, respectively.

4. Experimental campaign

Twenty-one FRCM-concrete joints with different geometrical characteristics, concrete surface preparation, and concrete mechanical properties are presented in this paper. The composite bonded length, composite bonded width, concrete block length, concrete batch (i.e. concrete substrate strength, see Table 1), and concrete surface preparation adopted for each specimen are summarized in Table 2. Specimens were named following the notation DS_X_Y_(U or W)_Z, where X = bonded length ℓ, in mm; Y = bonded width b_1, in mm; U indicates that the concrete surface was untreated; W indicates that concrete blocks with relatively low strength were used (i.e. concrete batch C employed, Table 1); and Z = specimen number.

Eleven specimens had a composite bonded length ℓ = 330 mm, whereas the remaining 10 had a bonded length ℓ = 450 mm. The bonded lengths employed are longer than the effective bond length l_{eff}, determined to be l_{eff} = 260 mm for this composite [26,27]. For 18 specimens, the concrete surface was simply cleaned from dust, referred to as untreated in the remainder of this paper, before the application of the FRCM composite (indicated by U in the specimen designation). The concrete prisms for these 18 specimens were constructed with concrete batch B. The concrete surface of the remaining three specimens was sandblasted, and the concrete prisms were constructed with lower strength concrete batch C (indicated by W in the specimen designation). A photo of the sandblasted surface is shown in Fig. 5a, and photos of the untreated concrete surfaces are shown in Fig. 5b and d. A composite bonded width b_1 = 60 mm was adopted for the three specimens with relatively low strength concrete blocks (concrete batch C), whereas two different composite bonded widths, namely 60 mm (9 specimens) and 80 mm (9 specimens) were adopted for specimens with higher strength concrete blocks (concrete batch B).

The results of the 21 tests presented in this paper were also compared with results previously obtained by the authors on PBO FRCM-concrete joints with a different concrete strength and surface preparation [25–27]. Thirty-nine specimens were selected for the comparison. Since a non-uniform load distribution along the bonded width was observed in FRCM-concrete joints tested using direct-shear set-ups [26,27,45], only the specimens that reported a relatively even load distribution among the fiber

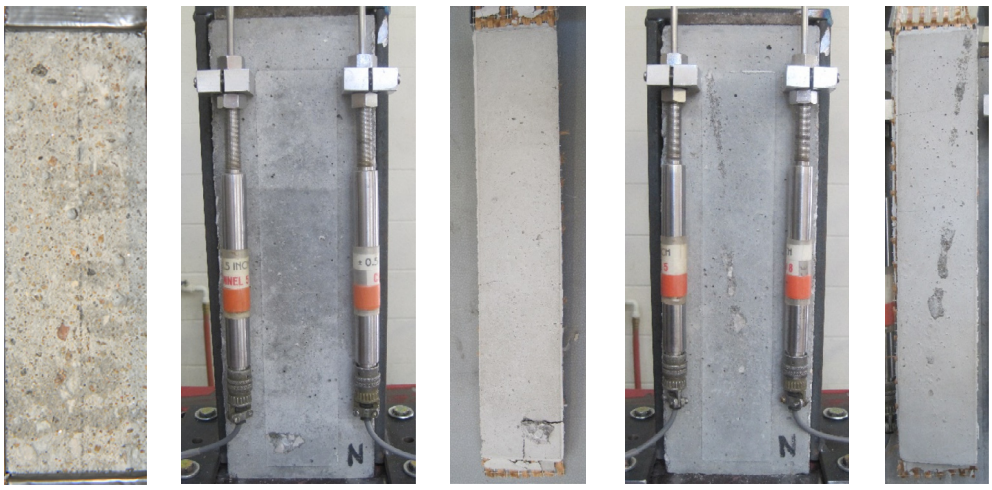

Fig. 5. (a) Concrete surface after sandblasting. Concrete surface (b) and composite strip (c) of specimen DS_330_60_U_1 after failure. Concrete surface (d) and composite strip (e) of specimen DS_330_60_U_2 after failure.

bundles [27] were considered reliable and used for the comparison. The criteria used to determine whether a specimen was reliable or not will be briefly recalled in Section 6.2. The selected (reliable) specimens, listed in Table 3, had a bonded length equal to 330 mm (26 specimens) and 450 mm (13 specimens) and bonded width equal to 43 mm (5 specimens), 60 mm (26 specimens), and 80 mm (8 specimens). The composite strips of specimens reported in Table 3 with bonded length equal to 330 mm and 450 mm were applied to concrete blocks constructed using concrete batches A and B, respectively (Table 1). For all specimens in Table 3, the con-crete surface was sandblasted before applying the composite. Specimens with bonded width equal to 34 mm were also tested [25,26] but were not considered because they presented a non-uniform distribution of the load among the different bundles and their peak loads were particularly scattered [27,46].

5. Experimental results

5.1. Peak load

The peak load value P^* (Fig. 2a) was recorded for each test specimen and was used to compute the peak stress σ^*:

$$\sigma^* = \frac{P^*}{nb^*t^*} \tag{3}$$

where n is the number of longitudinal fiber bundles within the composite bonded width. The values of the peak load and corresponding peak stress are reported in Tables 2 and 3 for each specimen.

5.2. Failure mode and load response

For the 21 FRCM-concrete joints presented in this paper and reported in Table 2, three different failure modes were observed: composite detachment (CD); fiber debonding (FD); and fiber failure (FF). The failure mode of each specimen is indicated in Table 2. All specimens reported in Table 3 failed due to debonding of the fibers (FD) from the embedding matrix.

The applied load–global slip curves of the series DS_330_60_U specimens are reported in Fig. 6a. The response of specimen DS_330_60_D_3, previously conducted by the authors and having a sandblasted concrete surface, is included for reference. The specimens of series DS_330_60_U exhibited shrinkage cracking of the matrix prior to loading. Specimens DS_330_60_U_1, DS_330_60_U_2, and DS_330_60_U_3 failed due to detachment of the entire composite strip from the concrete substrate. The failure was located at the composite–concrete interface, and detachment of the surface concrete was observed only for a very limited portion of the bonded area (Fig. 5b–e). This failure mode was previously observed by the authors for two specimens with bonded length ℓ = 100 mm (b_1 = 34 mm) and was attributed to the effect of the fracture mechanics Mode I condition that prevailed due to the short bonded length [25]. While specimens DS_330_60_U_1, 2, and 3 failed due to detachment of the entire composite strip, specimen DS_330_60_U_4 failed due to detachment of a portion of composite followed by debonding of the fibers within the embedding matrix. Further details about failure of specimen DS_330_60_U_4 are discussed in Section 6.1.

Specimen DS_330_60_U_3, which is not shown in Fig. 6a, failed due to detachment of the composite strip (Fig. 7a) at a very low applied load value. In this specimen the effect of the matrix shrinkage, which was more pronounced along the longitudinal direction (shrinkage cracks were orthogonal to the longitudinal direction), did not allow for proper bonding of the composite to the substrate, especially at the free end (Fig. 7b). The shrinkage of the matrix, combined with the poor matrix–concrete bond, led the composite strip to bend during the curing process preventing the adhesion of the composite to the substrate (Fig. 7b). This phenomenon was not observed in any of the other specimens tested by the authors.

The load responses of the series DS_330_80_U specimens are reported in Fig. 6b. The load response of specimen DS_330_80_D_1, previously conducted by the authors and having a sandblasted concrete surface, is included for comparison. Speci-mens of series DS_330_80_U failed by debonding of the fibers from the embedding matrix as described in Section 2. Debonding of the fibers along the entire bonded length was inferred from the longi-tudinal fibers that extended beyond the bonded length at the free end, which penetrated into the matrix (Fig. 8c and d). The applied load–global slip behavior of these specimens was affected by cracking of the matrix denoted by drops of the applied load (Fig. 6b). The peak load P^* of specimen DS_330_80_U_2 was lower than the peak load of other specimens with the same geometrical and mechanical characteristics, which was likely due to the broad matrix cracking pattern.

Specimen DS_330_80_U_4 presented several shrinkage cracks and, due to the opening of a major crack in the composite strip,

Table 2
Specimens tested.

Specimen	Concrete batch	Concrete block length L [mm]	Bonded length ℓ [mm]	Bonded width b_1 [mm]	Peak load P^* [kN]	Peak stress σ^* [MPa]	Failure mode	✓ or ✗
DS_330_60_U_1	B	375	330	60	3.60	1120	CD	✓
DS_330_60_U_2	B	375	330	60	3.67	1140	CD	✓
DS_330_60_U_3	B	375	330	60	0.70	220	CD	✗
DS_330_60_U_4	B	375	330	60	5.48	1700	CD/FD	✓
DS_330_80_U_1	B	375	330	80	8.91	2150	FD	✓
DS_330_80_U_2	B	375	330	80	5.96	1440	FD	✓
DS_330_80_U_3	B	375	330	80	9.25	2230	FD	✓
DS_330_80_U_4	B	375	330	80	7.48	1810	FD	✓
DS_450_60_U_1	B	510	450	60	7.07	2200	FD	✗
DS_450_60_U_2	B	510	450	60	7.33	2280	FD	✓
DS_450_60_U_3	B	510	450	60	7.28	2260	FD	✓
DS_450_60_U_4	B	510	450	60	6.80	2110	FD	✓
DS_450_60_U_5	B	510	450	60	6.54	2030	FD	✓
DS_450_80_U_1	B	510	450	80	9.47	2290	FD	✓
DS_450_80_U_2	B	510	450	80	8.40	2030	FD	✓
DS_450_80_U_3	B	510	450	80	8.69	2100	FD	✓
DS_450_80_U_4	B	510	450	80	10.01	2420	FD	✗
DS_450_80_U_5	B	510	450	80	8.86	2140	FD	✓
DS_330_60_W_1	C	375	330	60	6.45	2000	CD/FD	✓
DS_330_60_W_2	C	375	330	60	6.04	1880	CD/FD	✓
DS_330_60_W_3	C	375	330	60	6.43	2000	FD/FF	✓

Note: CD = composite detachment; FD = fiber debonding; FF = fiber failure outside the bonded area.

Table 3
Results of single-lap direct-shear tests previously conducted by the authors [25–27].

Specimen	Concrete batch	P^* [kN]	σ^* [MPa]	Failure mode	Specimen	Concrete batch	P^* [kN]	σ^* [MPa]	Failure mode
DS_330_43_2^T	A	5.25	2280	FD	DS_330_80_D_2	A	8.68	2100	FD
DS_330_43_3	A	5.27	2290	FD	DS_330_80_D_4	A	8.42	2030	FD
DS_330_43_6	A	5.09	2210	FD	DS_330_80_D_5	A	8.58	2070	FD
DS_330_43_S_2^T	A	5.12	2230	FD	DS_330_60_T_1	A	6.62	2060	FD
DS_330_43_S_3^T	A	3.03	1320	FD	DS_330_60_T_2	A	6.27	1950	FD
DS_330_60_1^T	A	7.05	2190	FD	DS_330_60_T_3	A	6.59	2050	FD
DS_330_60_2^T	A	6.56	2040	FD	DS_450_60_1	B	6.40	1990	FD
DS_330_60_3^T	A	6.06	1880	FD	DS_450_60_2	B	6.34	1970	FD
DS_330_60_4^T	A	6.50	2020	FD	DS_450_60_4	B	5.77	1790	FD
DS_330_60_5^T	A	6.28	1950	FD	DS_450_60_5	B	6.51	2020	FD
DS_330_60_D_1	A	8.29	2580	FD	DS_450_60_6	B	6.79	2110	FD
DS_330_60_D_2	A	7.12	2210	FD	DS_450_60_7	B	6.65	2070	FD
DS_330_60_D_3	A	6.56	2040	FD	DS_450_60_D_1	B	7.01	2180	FD
DS_330_60_D_4	A	5.24	1630	FD	DS_450_60_D_2	B	6.67	2070	FD
DS_330_60_D_5	A	6.69	2080	FD	DS_450_60_D_3	B	7.33	2280	FD
DS_330_60_S_2	A	7.31	2270	FD	DS_450_60_S_1	B	6.63	2060	FD
DS_330_60_S_3	A	6.55	2030	FD	DS_450_60_S_2	B	6.86	2130	FD
DS_330_80_1	A	8.47	2050	FD	DS_450_80_1	B	8.62	2080	FD
DS_330_80_3	A	8.28	2000	FD	DS_450_80_2	B	9.07	2190	FD
DS_330_80_D_1	A	8.90	2150	FD					

Note: S = presence of strain gauges mounted on the fiber net, D = specimen tested until a constant load at the end of the test was measured, T = transversal bundles removed before applying the matrix, superscript T = transversal fiber bundles oriented toward the concrete block [26].

shows a sudden drop in the P–g curve for a value of the applied load of approximately 6 kN (Fig. 6b). Photos of specimen DS_330_80_U_4 before and after the completion of the test are shown in Fig. 8c and d. The opening of a few major cracks in the matrix close to the loaded end (Fig. 8d) may have affected the peak load of specimen DS_330_80_U_4, which was slightly lower than the other specimens of the same series. The effects of the matrix cracks are further discussed in Section 6.1.

The load responses of series DS_450_60_U and series DS_450_80_U specimens are reported in Fig. 6c and d, respectively. Specimens DS_450_60_D_1 and DS_450_80_2, previously reported by the authors and having a sandblasted concrete surface, are also reported in Fig. 6c and d, respectively. Specimens of series DS_450_60_U failed due to debonding of the fibers from the embedding matrix as described in Section 2. The peak load values attained are similar to one another, although the peak loads for specimens DS_450_60_U_4 and 5 are slightly lower than the others of the same series. The initial slope of the P–g responses of the series DS_450_60_U specimens are slightly scattered likely due to stochastically distributed different matrix–fiber bond conditions [45] and to the presence of different matrix shrinkage crack patterns. This phenomenon was present in each specimen in each series, though it was more pronounced in some specimens. The slopes of the load responses of specimens DS_450_60_U_3–5 are similar up to a value of the global slip of approximately 0.6 mm. After that specimens DS_450_60_U_4 and 5 reported sudden drops of the applied load (Fig. 6c) caused by cracking of the matrix and damage at the matrix–fiber interface, which in turn resulted in a decrease of the P–g curve slope. These phenomena resulted in a lower value of the peak load P^* and a higher value of the global slip g corresponding to P^* with respect to other specimens in the same series.

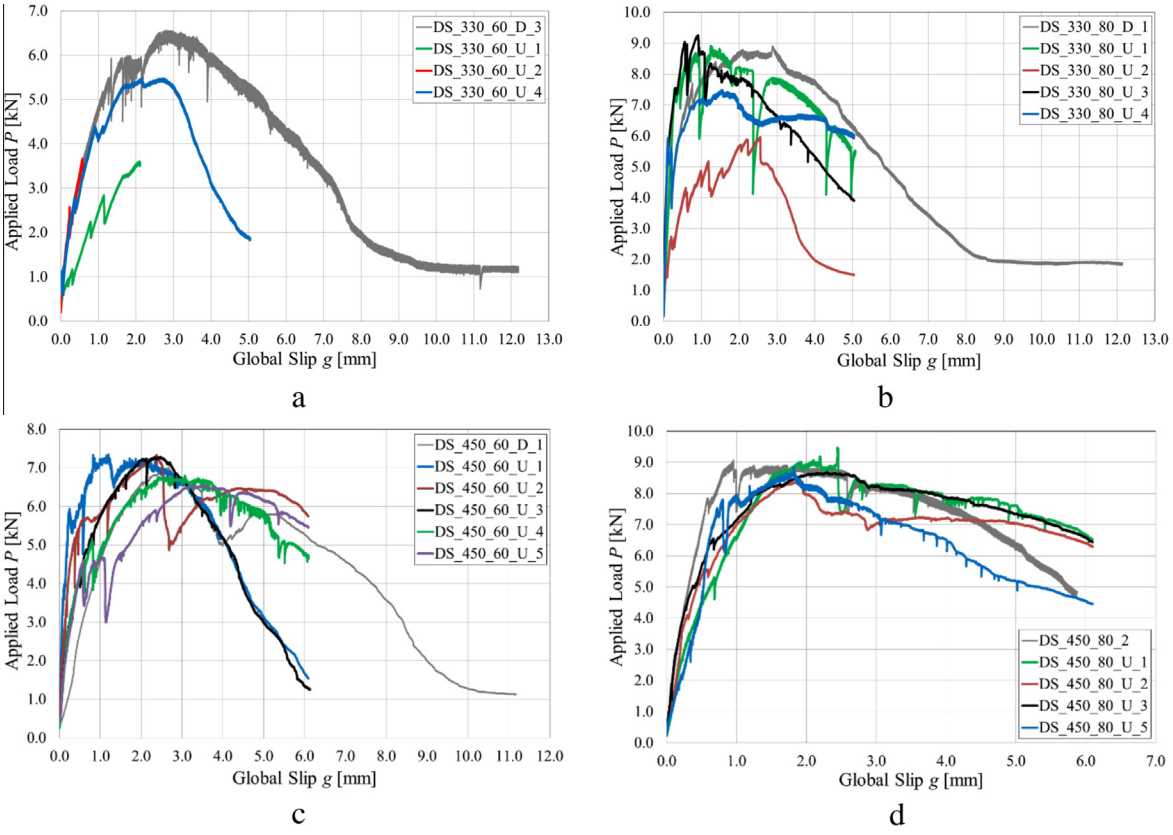

Fig. 6. (a) Load response of series DS_330_60_U specimens and specimen DS_330_60_D_3. (b) Load response of series DS_330_80_U specimens and specimen DS_330_80_D_1. (c) Load response of series DS_450_60_U specimens and specimen DS_450_60_D_1. (d) Load response of series DS_450_80_U specimens and specimen DS_450_80_2.

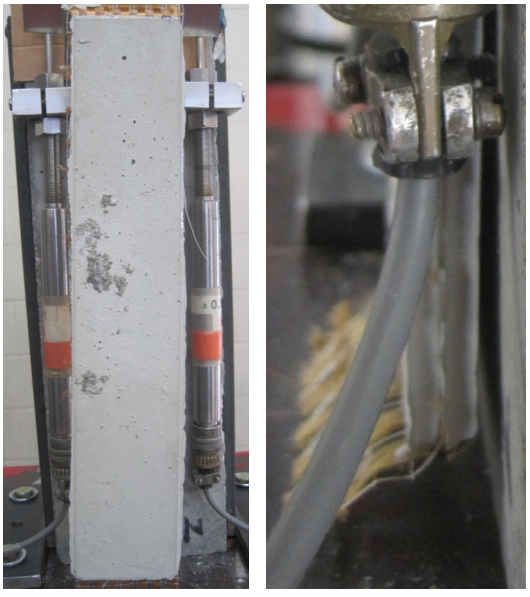

Fig. 7. Debonding (a) and detail of the shrinkage effect before the beginning of the test (b) of the composite strip of specimen DS_330_60_U_3.

Specimens of series DS_450_80_U failed due to debonding of the fiber from the embedding matrix (Fig. 6d). Their load responses resemble those observed for other specimens previously tested by the authors and described in Section 2, as can be observed by comparison with the applied load-global slip response of specimen DS_450_80_2 reported in Fig. 6d.

The load responses of the series DS_330_60_W specimens, which had a relatively low compressive strength of the substrate, are reported in Fig. 9. Specimen DS_330_60_D_3, which had a similar surface preparation but a higher concrete compressive strength, is included in Fig. 9 for comparison. Specimens in the DS_330_60_W series presented a mixed-mode failure. Specimens DS_330_60_W_1 and 2 failed due to detachment of a small portion of the composite from the concrete substrate near the loaded end, followed by debonding of the fibers from the embedding matrix. Failure of specimens DS_330_60_W_1 and 2 was similar to the failure observed in specimen DS_330_60_U_4. Detachment of a composite portion in specimens DS_330_60_W_1 and 2 caused sudden drops in the *P*–*g* curves for load values of approximately 3.8 kN (Fig. 9). Detachment of composite portions was initiated by through-thickness cracks in the matrix close to the loaded end (Fig. 10a) as discussed further in Section 6.1. After that, the fibers in the portion of composite that was still bonded to the con-crete substrate debonded at the matrix–fiber interface. After test-ing was completed, the detached composite portions in specimens DS_330_60_W_1 and 2 revealed small pieces of con-crete attached to the composite strips (Fig. 10b), which were not observed in composite strips that had detached from the substrate with higher concrete strength previously tested by the authors [25]. For specimen DS_330_60_W_3, one of the longitudinal fiber bundles failed outside the bonded area due to stress concentration. The rupture of the fiber bundle, which was located close to the edge of the composite strip (Fig. 10c), strongly affected the post-peak behavior of the specimen due to the uneven distribution of the applied load across the composite width, as will be further

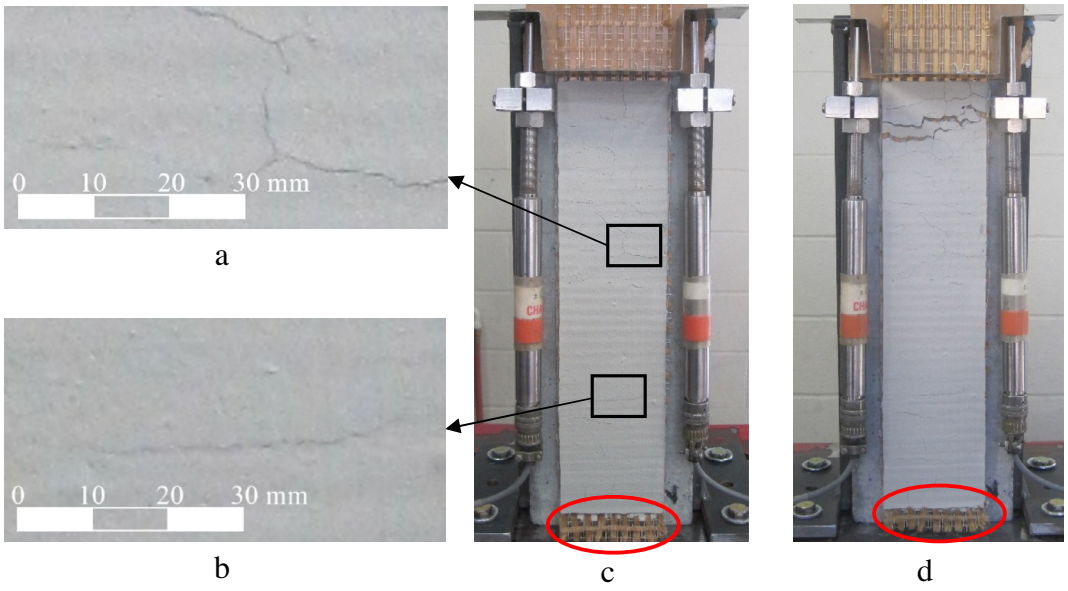

Fig. 8. Shrinkage cracks (a, b) of specimens DS_330_80_U_4 before testing. (c) Photo of the specimen before (c) and after (d) testing (note the penetration of the fiber at the free end inside the composite).

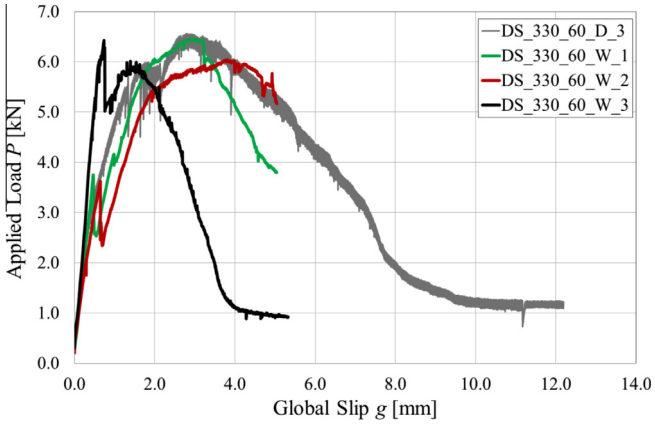

Fig. 9. Load response of series DS_330_60_W specimens and of specimen DS_330_60_D_3.

explained in Section 6.1. This phenomenon was observed in some specimens previously tested by the authors [25].

6. Discussion of results

6.1. Influence of the matrix cracks on the load response

Shrinkage cracks in the matrix were observed in several specimens presented in this paper (Section 5.2) and were previously observed by the authors in some FRCM-concrete joints comprised of the same type of matrix and fiber [25]. These cracks occurred shortly after casting the composite and before loading of the test specimen. The occurrence of shrinkage cracks depends on the matrix application and curing condition. The FRCM-concrete joints presented in this study and those previously tested by the authors [25–27] were cast under the same external conditions following the same procedure, although not all specimens presented shrinkage cracks. This suggests that the matrix utilized is sensitive to mixing, handling, or curing procedures, or a combination of these [25]. Some specimens exhibited a few shrinkage cracks with a prevalent transversal pattern, whereas a few specimens exhibited many shrinkage cracks spread over the matrix external surface without a predominant pattern. Position and orientation of shrinkage cracks did not appear to bear relation with position and orientation of the fiber bundles. The width of the shrinkage cracks was measured on images taken prior to testing and was found to vary from approximately 0.1 mm to 0.3 mm. As an example, Fig. 8a and b show shrinkage cracks with width of approximately 0.3 mm and 0.1 mm, respectively, exhibited on the external layer of matrix of specimen DS_330_80_U_4.

The presence of shrinkage cracks, which open with increasing global slip and result in a discontinuity in the stress-transfer between fibers and matrix, may affect the load response of the FRCM-concrete joint. In addition, formation of new cracks in the composite strip cause abrupt drops in the applied load. Shrinkage cracks, which are located on the external surface of the composite, may penetrate the thickness of the composite leading to debonding of portions of composite strip at the matrix-concrete interface.

A specific measure of the composite shrinkage was not performed during the experimental campaign described. Concrete shrinkage can be measured by measuring the length change in specimens subjected to a drying environment [47]. In the FRCM-concrete joints analyzed in this work, the restraining effect provided by bond at the concrete–composite interface did not allow length change of the strip at the interface, thus resulting in the formation of shrinkage cracks and hindering the measure of the composite shrinkage. Composite shrinkage is generally con-trolled by limiting the exposure of the composite to drying envi-ronment and, when that is difficult or not possible, by reinforcing the matrix with short fibers. Curing of polymer-modified matrices needs particular attention because exposure to a high-moisture environment may interfere with the polymerization process affecting the overall performance of the composite. Inorganic matrices used in FRCM composites should provide good bond with the fibers and the support and also have limited shrinkage. A procedure for characterizing FRCM composites, currently under investigation by different authors [16,17], could also include shrinkage measurement.

The load responses of series DS_330_60_U specimens were strongly affected by matrix cracking. Fig. 11a and b show the

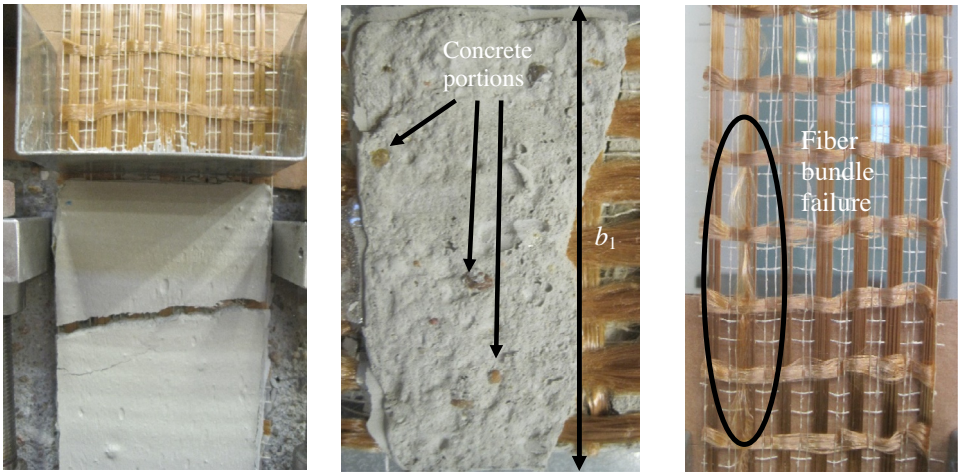

Fig. 10. (a) Through-thickness crack opening in specimen DS_330_60_W_1. (b) Matrix internal layer of specimen DS_330_60_W_1 detached during testing. (c) Failure of one fiber bundle in specimen DS_330_60_W_3.

evolution of the shrinkage cracks in specimen DS_330_60_U_4. The opening of cracks close to the loaded end that eventually penetrated the thickness of the composite, combined with the poor matrix–concrete bond, led a portion of the composite to detach from the concrete substrate (Fig. 11b and c). The detachment of a portion of the composite was followed by debonding of the fibers at the matrix–fiber interface. Since part of the composite detached from the substrate, the bonded length was reduced and, conse-quently, the peak load obtained was slightly lower than the peak loads of specimens in the same series.

The load responses of DS_330_60_W_1 and 2 were also influenced by through-thickness matrix cracks, which for these specimens were located close to the loaded end of the composite. Detachment of the composite from the concrete substrate, which was attributed to a fracture mechanics Mode I condition, was observed in specimens with a short bonded length (ℓ = 100 mm) previously tested by the authors [25]. It should be noted, however, that the substrate characteristics play a fundamental role in the failure mode affecting the composite–concrete stress-transfer mechanism. The detachment of a composite portion in specimens DS_330_60_W_1 and 2 could be due to the combined effect of fracture mechanics Mode I and II conditions associated with the relatively low mechanical properties of the concrete substrate for these specimens, although further study is needed to examine this effect.

The load response of specimen DS_330_80_U_2, for which the composite strip presented narrow shrinkage cracks, reported several drops of the applied load (Fig. 6b) corresponding to increasing crack opening. Fig. 12 shows the evolution of the crack pattern in specimen DS_330_80_U_2 for different points of the *P*–*g* curve. No detachment of the composite from the substrate was observed in specimen DS_330_80_U_2.

6.2. Influence of surface preparation

Tests previously conducted by the authors on FRCM-concrete joints with different composite widths showed that, although a width effect can be observed within a single fiber bundle [48], no width effect exists for the overall composite [26]. Nevertheless, the stochastically distributed properties of the matrix, local varia-tion of the bond characteristics of the fiber bundles, and perhaps a slight eccentricity of the applied load with respect to the composite width can cause a non-uniform distribution of the applied load in the different bundles. This phenomenon, which was evidenced by rigid rotation of the Ω-shape bent plate and by deformation of the bare transversal fiber bundles [25], can be evaluated by com-paring the displacement readings of the two LVDTs, namely LVDTa and LVDTb (Fig. 4a) used to control the test. Because the presence of a non-uniform load distribution may have a strong influence on the results obtained, the load response of each specimen needs to be analyzed to determine whether it can be considered reliable.

In order to assess the distribution of the load among bundles, the difference between the displacements measured by each LVDT, named g_a and g_b for LVDTa and LVDTb, respectively, was compared with the average value of the slip corresponding to the complete debonding of the fibers, $\bar{s}_f = 1.57$ mm (Fig. 3), computed through the fracture mechanics approach described in Section 2. Only specimens that reported a difference between the LVDTs lower than $\bar{s}_f$ for values of the applied load lower than the peak load P^* were considered reliable and are marked with a check symbol (✓) in Table 2. Specimens that were not considered reliable are marked with a cross symbol (✗) in Table 2. Table 3 includes all specimens in [26,27] that were determined to be reliable using this criterion.

As an example, the applied load *P* versus the global slip *g* and the displacements measured by the two LVDTs, g_a and g_b, of spec-imens DS_450_80_U_4 and DS_330_60_W_3 are reported in Fig. 13a and b, respectively. Specimen DS_450_80_U_4 reported an even distribution of the load among the different bundles, which is proven by the difference between the measurements of the two LVDTs that was much lower than the slip corresponding to complete debonding of the fibers during the entire test. Speci-men DS_330_60_W_3 (Fig. 13b) reported a substantial difference between the displacements measured by the two LVDTs for values of the global slip higher than approximately 2 mm, after the peak load P^* was attained. After attaining P^* one longitudinal fiber bundle located close to LVDTa (Fig. 10c) failed causing a non-uniform load distribution [27]. LVDTb measured displacements up to approximately 10 mm whereas LVDTa measured negative displacements, which correspond to null contribution of the bundles close to LVDTa, due to rigid rotation of the Ω-shape bent plate. It should be noted that the displacement measured by LVDTb attained values that, in terms of global slip *g*, correspond to a constant load due to friction, as can be observed in specimen DS_330_60_D_3 (Fig. 9). Fiber bundles close to LVDTb, which underwent substantial displacement, completely debonded from the matrix resulting in a constant applied load value.

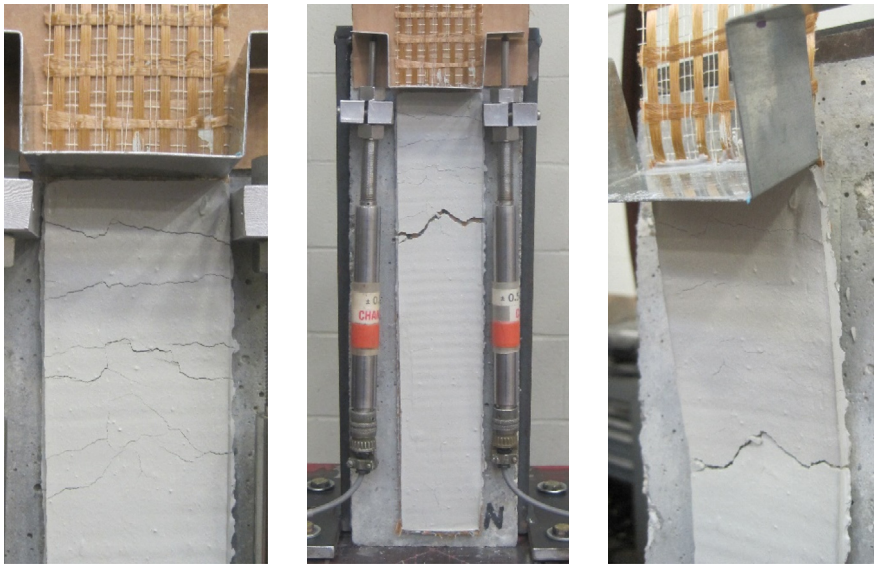

Fig. 11. Opening of matrix shrinkage cracks (a, b) and consequent debonding of a portion of the composite (c) in specimen DS_330_60_U_4.

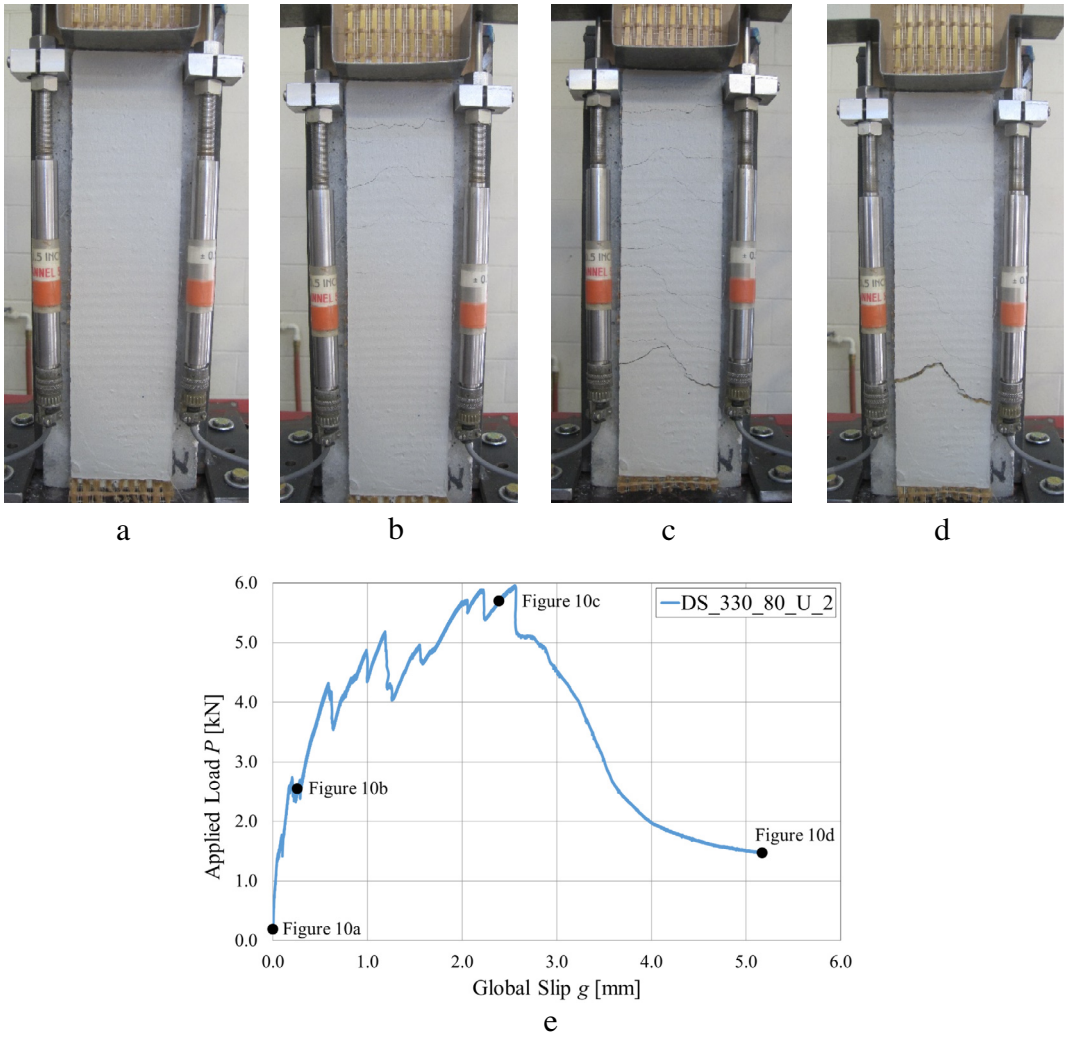

Fig. 12. Crack pattern evolution during testing (a–d) and corresponding applied load values (e) of specimen DS_330_80_U_2.

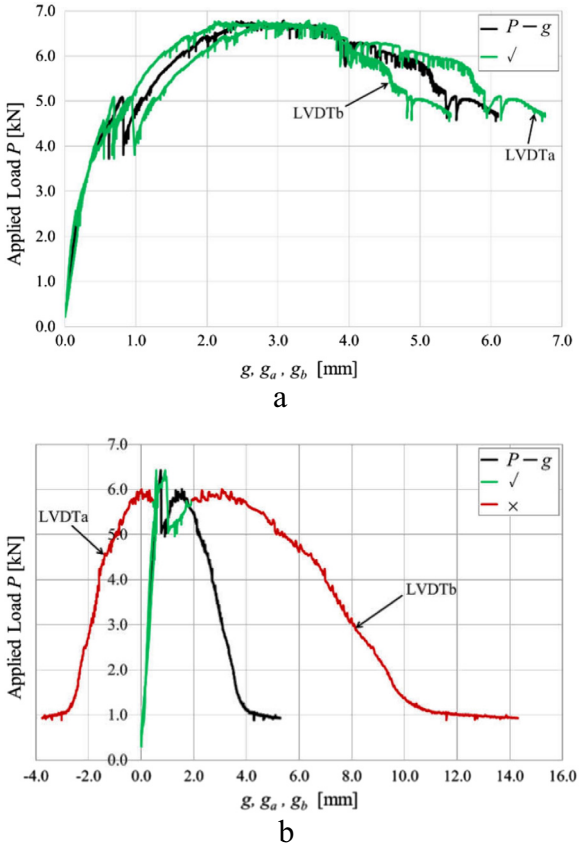

Fig. 13. Applied load vs. LVDT measurements for specimens (a) DS_450_80_U_4 and (b) DS_330_60_W_3.

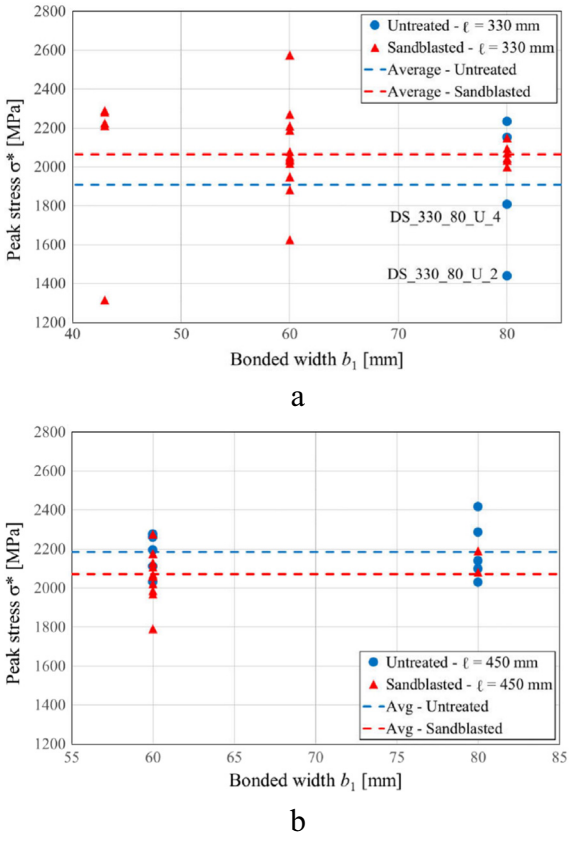

Fig. 14. Peak stress σ^* vs. bonded width b_1 for specimens with concrete surface sandblasted and untreated with composite bonded length (a) ℓ = 330 mm and (b) ℓ = 450 mm.

To examine the influence of concrete strength, the load responses of specimens in series DS_330_60_W were compared with those of specimens with the same composite characteristics and applied to concrete blocks with a higher concrete strength (i.e. concrete batch A; concrete batch B was used only for speci-mens with bonded length ℓ = 450 mm). Although all specimens in series DS_330_60_W were determined to be reliable (Table 2), specimen DS_330_60_W_3 will not be considered in the following comparison because one of the fiber bundles failed, potentially affecting P^*. Since the composite portions detached in specimens DS_330_60_W_1 and 2 were small compared to the bonded length, it is assumed that the peak load values obtained were not strongly affected and can be representative of the specimens in this series. The values of P^* obtained from specimens of series DS_330_60_W are similar to those obtained by specimens with the same characteristics and concrete blocks with higher strength (see Tables 2 and 3, and Fig. 9). The average peak stress of specimens of series DS_330_60_W was computed to be $\bar{\sigma}^*_{330\,W}$ = 1940 MPa. The aver-age peak stress of specimens in Table 3 with a bonded length of 330 mm and a higher concrete strength was computed to be $\bar{\sigma}^*_{330}$ = 2060 MPa, with a difference of approximately 6%. Compar-ison of the peak stress, applied load-global slip behavior (Fig. 9), and failure mode of the DS_330_60_W specimens with specimens reported in Table 3 suggests that the strength of the concrete block did not influence the response of the FRCM-concrete joint. How-ever, further study is needed to confirm these results with con-cretes of lower strengths than those employed in this paper.

To examine the influence of surface preparation, Fig. 14a and b show the peak stress σ^* for specimens with bonded length ℓ = 330 mm and ℓ = 450 mm, respectively, reported in Tables 2 and 3. Only specimens that failed due to fiber debonding (FD) and that were considered reliable (i.e. reported an even distribution of the load among bundles) were considered in Fig. 14. Specimen DS_330_60_U_4 was not considered because it failed due to composite detachment (CD) followed by fiber debonding (FD). Specimens of series DS_330_60_W were not considered in Fig. 14.

The average peak stress values obtained for specimens with bonded length ℓ = 330 mm and ℓ = 450 mm and for which the concrete surface was not sandblasted before applying the composite are $\bar{\sigma}^*_{330\,U}$ = 1910 MPa and $\bar{\sigma}^*_{450\,U}$ = 2190 MPa, respectively. The average peak stress values obtained for specimens with bonded length ℓ = 330 mm and ℓ = 450 mm and for which the concrete surface was sandblasted is equal to $\bar{\sigma}^*_{330}$ = 2060 MPa and $\bar{\sigma}^*_{450}$ = 2070 MPa, respectively. The average peak stress values obtained are higher for treated than for untreated specimens with ℓ = 330 mm (7% difference), whereas they are higher for untreated than for treated specimens for ℓ = 450 mm (5% difference). Further-more, it should be noted that the average peak stress value com-puted for untreated specimens with bonded length ℓ = 330 mm, $\bar{\sigma}^*_{330\,U}$, includes the results of specimens whose load responses were affected by the presence of shrinkage cracks and were lower than others within the same series, namely DS_330_80_U_2 and 4 (identified in Fig. 14a, see Section 6.1). The results obtained indicate that the concrete surface preparation plays a limited role in the FRCM-concrete joint peak load and load response. However, it should be noted that poor bond between the composite and the untreated surface combined with the presence of matrix shrinkage cracks influenced the failure mode in four specimens. In order to avoid the possibility of sudden composite detachment failure, a proper application of the composite should be performed, and the matrix shrinkage should be controlled.

The conclusions drawn regarding the influence of the concrete strength and surface preparation are valid when a single layer of fiber is employed. When more layers of fiber are employed the failure mode may change from the matrix–fiber interface to the concrete–composite interface [6,49]. In this case the substrate characteristics may play a fundamental role in the behavior of the FRCM-concrete joint.

7. Conclusions

The results obtained from 21 single-lap direct-shear tests conducted on PBO FRCM-concrete joints with two different bonded lengths and two different bonded widths were presented in this paper. The concrete surface onto which the FRCM composite strip was applied was simply cleaned (otherwise untreated) for 18 specimens, whereas it was sandblasted for the remaining three. The three specimens for which the concrete surface was sandblasted included a concrete substrate that had a relatively low compressive strength. Findings are summarized as follows:

- Different failure modes were observed, namely debonding of the fibers at the matrix–fiber interface, detachment of the composite at the concrete–composite interface, and fiber failure (rupture) outside the bonded length. Detachment of the entire composite or portion of it from the concrete substrate was observed for four specimens that were not subjected to surface preparation except for cleaning. The failure was attributed to poor bond at the concrete–composite interface combined with the presence of matrix shrinkage cracks.
- Fourteen specimens with an untreated concrete surface failed due to fiber debonding at the matrix–fiber interface. The load responses obtained were compared with those previously obtained by the authors for other FRCM-concrete joints with the same geometrical characteristics and a treated (sandblasted) concrete surface, showing that the surface preparation has a limited role in the behavior of the FRCM-concrete joint, provided that the matrix shrinkage is controlled.
- Three FRCM-concrete joints that were cast on concrete blocks with relatively low concrete strength presented mixed-mode failures. Two specimens failed due to detachment of a portion of composite followed by fiber debonding at the matrix–fiber interface, whereas one specimen failed due to fiber debonding followed by rupture of a fiber bundle outside the bonded length. These failure modes were influenced by the presence of matrix shrinkage cracks and by the distribution of the applied load among the longitudinal bundles. Although the peak load values obtained were consistent with the values reported by specimens with the same characteristics and higher strength concrete blocks, further study is needed to confirm these results with concretes of lower strengths than those employed in this paper.
- In order to avoid the possibility of sudden composite detachment failure, the authors recommend that the substrate surface should be treated, and the matrix shrinkage should be controlled.

Acknowledgements

The experimental work discussed in this paper was conducted at Missouri University of Science and Technology (Missouri S&T). The authors would like to express their appreciation to the National University Transportation Center (NUTC) at Missouri S&T for providing financial support for this project. Ruredil S.p.A. of San Donato Milanese, Italy, is gratefully acknowledged for providing the composite materials.

References

[1] L.A. Bisby, T.J. Stratford, E.C. Roy, M. Ward, Fibre reinforced cementitious matrix systems for fire-safe flexural strengthening of concrete: pilot testing at ambient temperatures, in: Proceedings of Advanced Composites in Construction Conference (ACIC), NetComposites Ltd, 2009, pp. 449–460.
[2] I. Del Prete, A. Bilotta, E. Nigro, Performance at high temperature of RC bridge decks strengthened with EBR-FRP, Compos. Part B 68 (2015) 27–37.
[3] C. Pellegrino, T. D'Antino, Experimental behaviour of existing precast prestressed reinforced concrete elements strengthened with cementitious composites, Compos. Part B 55 (2013) 31–40.
[4] L. Ombres, Debonding analysis of reinforced concrete beams strengthened with fibre reinforced cementitious mortar, Eng. Fract. Mech. 81 (2012) 94–109. A.
[5] D'Ambrisi, F. Focacci, L. Raimondo, V. Alecci, M. De Stefano, Carbon FRCM materials for structural upgrade of masonry arch and road bridges, Compos. Part B (2015), http://dx.doi.org/10.1016/j.compositesb.2015.01.024.
[6] A. D'Ambrisi, F. Focacci, Flexural strengthening of RC beams with cement based composites, J. Compos. Constr. 15 (2) (2011) 707–720.
[7] A. D'Ambrisi, F. Focacci, A. Caporale, Strengthening of masonry-unreinforced concrete railway bridges with PBO-FRCM materials, Compos. Struct. 102 (2013) 193–204.
[8] T.C. Triantafillou, C.G. Papanicolaou, Shear strengthening of reinforced concrete members with textile reinforced mortar (TRM) jackets, Mater. Struct. 39 (2006) 93–103.
[9] T. Blanksvärd, B. Täljsten, A. Carolin, Shear strengthening of concrete structures with the use of mineral-based composites, J. Compos. Constr., ASCE 13 (1) (2009) 25–34.
[10] E. Tzoura, T.C. Triantafillou, Shear strengthening of reinforced concrete T-beams under cyclic loading with TRM or FRP jackets, Mater. Struct. (2014), http://dx.doi.org/10.1617/s11527-014-0470-9.
[11] L. Ombres, Structural performance of reinforced concrete beams strengthened in shear with a cement based fiber composite material, Compos. Struct. 122 (2015) 316–329.
[12] T.C. Triantafillou, C.G. Papanicolaou, P. Zissimopoulos, T. Laourdekis, Concrete confinement with textile-reinforced mortar jackets, ACI Struct. J. 103 (1)(2006) 28–37.
[13] D. Bournas, P. Lontou, C.G. Papanicolaou, T.C. Triantafillou, Textile-reinforced mortar (TRM) versus FRP confinement in reinforced concrete columns, ACI Struct. J. 104 (6) (2007) 740–748.
[14] D.A. Bournas, T.C. Triantafillou, K. Zygouris, F. Stavropoulos, Textile-reinforced mortar (TRM) versus FRP jacketing in seismic retrofitting of RC columns with continuous or lap-spliced deformed bars, J. Compos. Constr. 13 (5) (2009) 360–371.
[15] L. Ombres, Concrete confinement with a cement based high strength composite material, Compos. Struct. 109 (2014) 294–304.
[16] F.G. Carozzi, C. Poggi, Mechanical properties and debonding strength of fabric reinforced cementitious matrix (FRCM) systems for masonry strengthening, Compos. Part B 70 (2015) 215–230.
[17] F. De Santis, G. De Felice, Tensile behaviour of mortar based composites for externally bonded reinforcement systems, Compos. Part B 68 (2015) 401–413.
[18] American Concrete Institute (ACI), Guide for the design and construction of externally bonded FRP systems for strengthening of concrete structure, ACI 440.2R-08, Farmington Hill, Michigan, 2008.
[19] C. Pellegrino, D. Tinazzi, C. Modena, An experimental study on bond behavior between concrete and FRP reinforcement, J. Compos. Constr., ASCE 12 (2) (2008) 180–189.
[20] A. D'Ambrisi, L. Feo, F. Focacci, Bond-slip relations for PBO-FRCM materials externally bonded to concrete, Compos. Part B 43 (8) (2012) 2938–2949.
[21] A. D'Ambrisi, L. Feo, F. Focacci, Experimental analysis on bond between PBO-FRCM strengthening materials and concrete, Compos. Part B 44 (1) (2013) 524–532.
[22] S. Hashemi, R. Al-Mahaidi, Experimental and finite element analysis of flexural behavior of FRP-strengthened RC beams using cement-based adhesives, Constr. Build. Mater. 26 (2012) 268–273.
[23] C.T.M. Tran, B. Stitmannaithum, T. Ueda, Investigation of the bond behavior between PBO-FRCM strengthening material and concrete, J. Adv. Concr. Tech. 12 (2014) 545–557.
[24] A. D'Ambrisi, L. Feo, F. Focacci, Experimental and analytical investigation on bond between carbon-FRCM materials and masonry, Compos. Part B 46 (2013) 15–20.
[25] L.H. Sneed, T. D'Antino, C. Carloni, Investigation of bond behavior of PBO fiber-reinforced cementitious matrix composite–concrete interface, ACI Mater. J. 111 (5) (2014) 569–580.
[26] T. D'Antino, C. Carloni, L.H. Sneed, C. Pellegrino, Matrix–fiber bond behavior in PBO FRCM composites: a fracture mechanics approach, Eng. Fract. Mech. 117 (2014) 94–111.
[27] C. Carloni, T. D'Antino, L.H. Sneed, C. Pellegrino, Role of the matrix layers in the stress-transfer mechanism of FRCM composites bonded to a concrete substrate, J. Eng. Mech, ASCE (2014), http://dx.doi.org/10.1061/(ASCE)EM.1943-7889.0000883.
[28] B. Banholzer, T. Brockmann, W. Brameshuber, Material and bonding characteristics for dimensioning and modeling of textile reinforced concrete (TRC) elements, Mater. Struct. 39 (2006) 749–763.
[29] R. Ortlepp, S. Ortlepp, M. Curbach, Stress transfer in the bond joint of subsequently applied textile reinforced concrete strengthening, in: Proc. Fibre-Reinforced Concretes (FRC), RILEM, PRO 39, Varenna, Italy, 2004.

[30] R. Ortlepp, U. Hampel, M. Curbach, A new approach for evaluating bond capacity or TRC strengthening, Cem. Concr. Compos. 28 (2006) 589–597.
[31] M. Curbach, R. Ortlepp, T.C. Triantafillou, TRC for rehabilitation, in: W. Brameshuber (Ed.), Textile Reinforced Concrete, RILEM Report 36, 2006, pp. 221–236.
[32] T. D'Antino, C. Pellegrino, C. Carloni, L.H. Sneed, Experimental analysis of the bond behavior of glass, carbon, and steel FRCM composites, Key Eng. Mater. 624 (2015) 371–378.
[33] C. Carloni, K.V. Subramaniam, Direct determination of cohesive stress transfer during debonding of FRP from concrete, Compos. Struct. 93 (1) (2010) 184–192.
[34] J. Yao, J.G. Teng, J.F. Chen, Experimental study on FRP-to-concrete bonded joints, Compos. Part B 36 (2005) 99–113.
[35] C. Carloni, K.V. Subramaniam, Investigation of sub-critical fatigue crack growth in FRP/concrete cohesive interface using digital image analysis, Compos. Part B 51 (2013) 35–43.
[36] Z.P. Bazant, J. Planas, Fracture and Size Effect in Concrete and Other Quasi-Brittle Materials, CRC Press, Boca Raton, Florida, 1997.
[37] T. D'Antino, Bond behavior in fiber reinforced polymer composites and fiber reinforced cementitious matrix composites (Ph.D. thesis), Univ. of Padova, Padova, Italy, 2014.
[38] P. Carrara, D. Ferretti, F. Freddi, G. Rosati, Shear tests of carbon fiber plates bonded to concrete with control of snap-back, Eng. Fract. Mech. 78 (15) (2011) 2663–2678.
[39] C. Carloni, T. D'Antino, L.H. Sneed, C. Pellegrino, An investigation of PBO FRCM-concrete joint behavior using a three-dimensional numerical approach, in: Proc. 15th International Conference on Civil, Structural, and Environmental Engineering Computing, 1–4 Sept 2015, Prague, Czech Republic.
[40] T. D'Antino, C. Pellegrino, C. Carloni, L.H. Sneed, Numerical analysis of PBO FRCM-concrete joints, in: Proc. 12th International Symposium on Fiber Reinforced Polymers for Reinforced Concrete Structures (FRPRCS12), 14–16 Dec 2015, Nanjing, China.
[41] ASTM D3039/D3039M-08, Standard Test Method for Tensile Properties of Polymer Matrix Composite Materials, ASTM International, West Conshohocken, PA, 2008, 13 p.
[42] T. D'Antino, L.H. Sneed, C. Carloni, C. Pellegrino, Bond behavior of the FRCM-concrete interface, in: Joaquim Barros, José Sena-Cruz (Eds.), Proc. XI Int. Symp. on Fiber Reinforced Polymers for reinforced Concrete Structures (FRPRCS11), 2013.
[43] ASTM C39/C39M-12, Standard Test Method for Compressive Strength for Cylindrical Concrete Specimens, ASTM International, West Conshohocken, PA, 2012, 7 pp.
[44] ASTM C496/C496M-11, Standard Test Method for Splitting Tensile Strength of Cylindrical Concrete Specimens, ASTM International, West Conshohocken, PA, 2011, 5 pp.
[45] L.H. Sneed, T. D'Antino, C. Carloni, C. Pellegrino, A comparison of the bond behavior of PBO-FRCM composites determined by single-lap and double-lap shear tests, Cem. Concr. Compos. http://dx.doi.org/10.1016/j.cemconcomp.2015.07.007.
[46] T. D'Antino, C. Carloni, L.H. Sneed, C. Pellegrino, Fatigue and post-fatigue behavior of PBO FRCM-concrete joints, Int. J. Fatigue. http://dx.doi.org/10.1016/j.ijfatigue.2015.06.008.
[47] M. Grzybowski, S. Shah, Shrinkage cracking of fiber reinforced concrete, ACI Mater. J. 87 (2) (1990) 138–148.
[48] B. Banholzer, Bond behavior of multi-filament yarn embedded in a cementitious matrix (PhD Thesis), RETH Aachen University, United Kingdom, 2004.
[49] G. Loreto, L. Leardini, D. Arboleda, A. Nanni, Performance of RC slab-type elements strengthened with fabric reinforced cementitious matrix composites, J. Compos. Constr. 18 (3) (2013) 1–9.